AGU PUBLICATIONS

JGR

Journal of Geophysical Research: Atmospheres

RESEARCH ARTICLE
10.1002/2016JD025170

Key Points:
- Crosstalk effect may have strong impact on nonlinear calibration coefficients
- Crosstalk correction algorithm is applied to correct the crosstalk effect
- Crosstalk correction rectifies the higher-order calibration

Crosstalk effect mitigation in black body warm-up cool-down calibration for Terra MODIS longwave infrared photovoltaic bands

Junqiang Sun[1,2], Sriharsha Madhavan[1,3], and Menghua Wang[1]

[1]Center for Satellite Applications and Research, E/RA3, NOAA National Environmental Satellite, Data, and Information Service, College Park, Maryland, USA, [2]Global Science and Technology, Greenbelt, Maryland, USA, [3]Science Systems and Applications Inc., Lanham, Maryland, USA

Correspondence to:
J. Sun,
junqiang.sun@noaa.gov

Citation:
Sun, J., S. Madhavan, and M. Wang (2016), Crosstalk effect mitigation in black body warm-up cool-down calibration for Terra MODIS longwave infrared photovoltaic bands, *J. Geophys. Res. Atmos.*, *121*, 8311–8328, doi:10.1002/2016JD025170.

Received 31 MAR 2016
Accepted 7 JUL 2016
Accepted article online 12 JUL 2016
Published online 27 JUL 2016

Abstract The crosstalk phenomena in Terra MODerate-resolution Imaging Spectroradiometer (MODIS) midwave-to-longwave infrared (LWIR) photovoltaic (PV) bands (bands 27-30) have recently been individually studied and characterized, and a correction algorithm has been developed. The routine calibration of the four LWIR PV bands uses an onboard black body (BB) based on a quadratic model for the relationship between the at-aperture radiance and the background subtracted instrument response. While the crosstalk correction has been successfully applied in both the routine BB calibration (scan basis) to correct the crosstalk effect in the linear term and the Earth view (EV) radiance in our previous investigations on the bands 27–29, the most recent work on band 30 demonstrated a newfound necessity to include the impact of the crosstalk effect on the nonlinear term as well as the offset. In this paper, we analyze the calibration calculation under a variety of conditions consistent with the MODIS Collection 6 settings to examine the impact of the crosstalk effect in the two terms derived from the BB warm-up-cool-down (WUCD) calibration. We show that with correct account of the crosstalk effect in the WUCD calibration, the sudden changes and other abnormal features that have been observed in the two terms for many years are effectively and remarkably removed. In addition, imagery for bands 27–29 using the calibration result fully corrected for the electronic crosstalk effect shows further improvement over previous results that account for only the corrected linear term, whereas for the band 30 different testing scenes validate the previous fully corrected findings.

1. Introduction

The MODerate-resolution Imaging Spectroradiometer (MODIS), a stupendous sensor in the fleet of Earth Observing System (EOS) for the National Aeronautics and Space Administration (NASA), is in space orbit on two spacecrafts, Terra (T) and Aqua (A) [*Barnes and Salomonson*, 1993; *Salomonson et al*., 2002; *Guenther et al*., 2002; *Justice et al*., 1998; *Esaias et al*., 1998; *King et al*., 2003, and *Parkinson*, 2013]. They have been on orbit for more than 16 and 14 years, respectively. MODIS is a whiskbroom scanning radiometer that includes a 360° rotating double-sided scan mirror and several onboard calibrators (OBCs) as illustrated in Figure 1. The MODIS instruments remotely capture the top of atmosphere radiance from the Earth in 36 spectral bands varying from 0.41 μm to 14.4 μm. The spectral wavelengths from 3.7 μm onward cover the thermal infrared region which is interspaced into 16 thermal emissive bands (TEBs). The key design parameters including the calibration requirements for the detector noise and the primary application for each of the TEBs are listed in Table 1. The TEBs are located on the short and middle wave infrared Focal Plane Assembly (FPA) and the longwave infrared (LWIR) FPA as shown in Figure 2 with red outline highlighted. The TEBs are calibrated on orbit by the onboard black body (BB) shown in Figure 1 with highlight as well [*Xiong et al*., 2008, 2009, and 2015].

A quadratic model for the relationship between the at-aperture radiance and the background subtracted instrument response is applied to MODIS TEBs [*Xiong et al*., 2009], wherein the linear term has major contribution and the offset and nonlinear terms are minor contributors. However, they can become important when the sensor's operating range deviates significantly from the linear range, i.e., when the radiance levels are at well below 0.3 $L_{typical}$, the typical scene radiance, or close to L_{max}, the maximum radiance, respectively. The coefficients of the quadratic form are called calibration coefficients. They are extracted on a quarterly basis through a multiday temperature-controlled BB warm-up cool-down (WUCD) process covering the

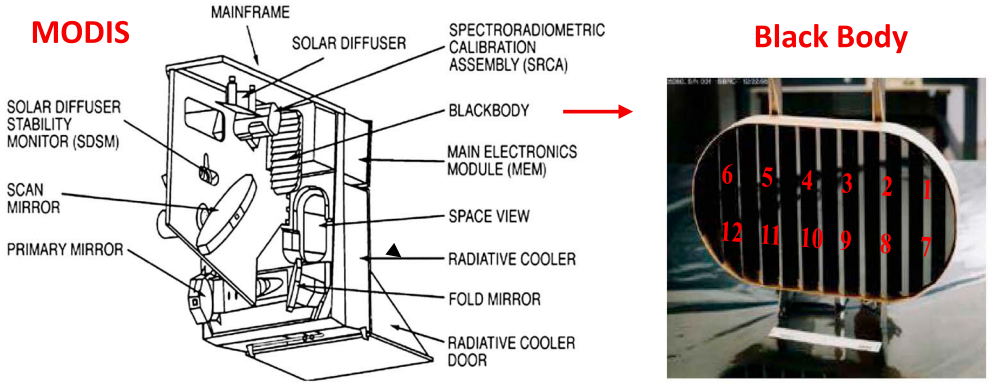

Figure 1. MODIS instrument setup with onboard calibrators.

temperature range of about 270 K to 315 K [*Xiong et al*., 2009]. From each BB WUCD data a quadratic fit is applied to extract the offset, a_0, the linear term, a_1, and the nonlinear term, a_2. In between two quarterly WUCD events, the linear term is updated on a scan-by-scan basis from routine BB calibration with offset and linear terms fixed. The BB temperature is controlled at 290 K for Terra (T) MODIS and 285 K for Aqua (A) MODIS, respectively, for routine BB calibration [*Xiong et al*., 2009].

Among 16 TEBs, there are four LWIR photovoltaic (PV) bands from 6.7 μm to 9.7 μm (bands 27–30). In their calibration coefficients, i.e., offset, linear, and nonlinear terms, derived from the WUCD and routine BB calibration, unexpected sudden jumps and rapid changes have been seen in all three terms since early in mission. These features become increasingly more dramatic after the instruments passed the designed lifetime (6 years) [*Xiong et al*., 2015]. These features are strongly detector dependent, which results in large detector differences in calibration coefficients, and gave rise to severe striping in Earth view (EV) L1B products, especially in the last several years. The features are also band dependent. Recently, *Sun et al*. [2011, 2014a, 2014b, 2014c, 2015a, 2015b, 2015c, 2016] and *Madhavan et al*. [2014, 2015] have shown that these four bands have suffered from degradation in the electronic circuits causing signal leaks among their circuitries. They have developed a linear theory and correction algorithm to characterize and mitigate the crosstalk effect and have intensively studied the crosstalk phenomena in the four LWIR PV bands. At the first order, the crosstalk correction is only applied to the routine BB calibration and the Earth view (EV) radiance and demonstrated to work remarkably well in the previous investigations on bands 27–29 [*Sun et al*., 2011, 2014a, 2014b, 2014c, 2015a, 2015b, 2015c]. The direct application of crosstalk correction suffices for these three bands without needing to reanalyze the offset term and the nonlinear term through the full WUCD

Table 1. MODIS Spectral Band Design Specifications[a]

TEB Band	CW	BW	Ttyp	NEdT	Primary Use
20	3.75	0.18	300	0.05	Surface/cloud temperature
21	3.96	0.06	335	0.20	
22	3.96	0.06	300	0.07	
23	4.05	0.06	300	0.07	
24	4.47	0.07	250	0.25	Atmospheric temperature
25	4.52	0.07	275	0.25	
27	6.72	0.36	240	0.25	Water vapor
28	7.33	0.30	250	0.25	
29	8.55	0.30	300	0.05	Cloud properties
30	9.73	0.30	250	0.25	Ozone
31	11.03	0.50	300	0.05	Surface/cloud temperature
32	12.02	0.50	300	0.05	
33	13.34	0.30	260	0.25	Cloud top altitude
34	13.64	0.30	250	0.25	
35	13.94	0.30	240	0.25	
36	14.24	0.30	220	0.35	

[a]CW is center wavelength in μm; BW is bandwidth in μm; Ttyp is typical temperature in K; NEdT is noise equivalent difference temperature in K.

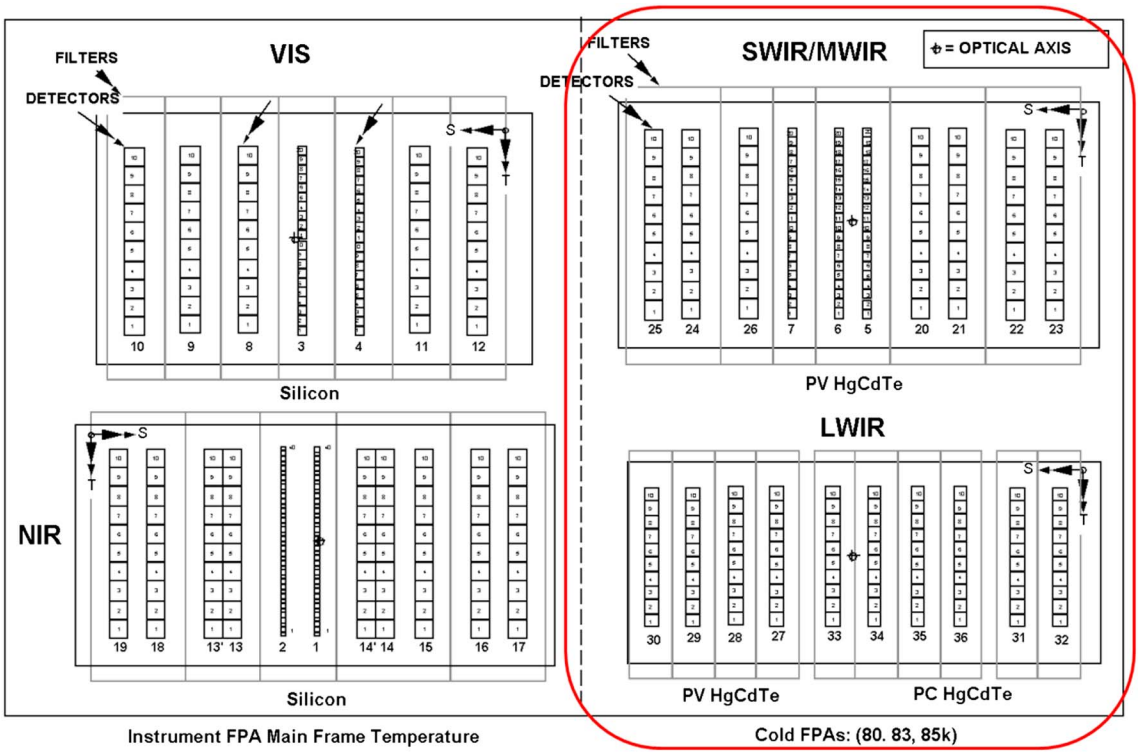

Figure 2. MODIS Focal Plane layout (red box highlighting the TEB).

calculation. The crosstalk correction rectified the linear calibration term for the various detectors on three counts. First, the differences among the linear terms for the detectors of each given band were significantly reduced. Second, the sudden jumps in the linear terms were greatly curtailed. Third, the long-term sharp drifting pattern in the linear terms was largely moderated. Consequently, the EV retrievals showed improvements and significant reduction of striping artifacts due to the detector responses being well balanced. *Sun et al*. [2014b, 2015a, 2015c] have also found that there are long-term radiometric drifts in Collection 6, the most recent version of L1B, EV retrievals and shown that the crosstalk correction can remove or significantly reduce the long-term radiometric drifts, leading to a very stable lifetime trend.

While the crosstalk correction has been successfully applied in both the routine BB calibration (scan-by-scan basis) to correct the crosstalk effect in the linear term and the EV radiance in our previous works on bands 27–29 [*Sun et al*., 2011, 2014a, 2014b, 2014c, 2015a, 2015b, 2015c], the most recent work on the band 30 explicitly demonstrated a newfound necessity to include the impact of the crosstalk effect on the nonlinear term as well as the offset, which indicated that the crosstalk correction is required to be applied to the WUCD calibration for the Terra band 30 [*Sun et al*., 2016]. As mentioned above, the unexpected sudden jumps and rapid increases have been observed in the nonlinear term for many years, although these unexpected abnormal phenomena were not understood. With the realization that the investigation of the crosstalk effect needs to delve deeper into the WUCD calibration, we analyze the calibration calculation under a variety of conditions consistent with the official MODIS Collection 6 settings [*Wenny et al*., 2012b; *Xiong et al*., 2013]. No electronic crosstalk correction has ever been applied to any components of the official MODIS L1B C6 or any earlier MODIS L1B version. In this paper, we will show that with the correction accounting for the crosstalk effect in the offset and quadratic calibration terms in the retrieval algorithms, the sudden changes and other unexpected abnormal features that have been observed in the two terms as aforementioned are effectively and remarkably removed. It is here revealed and understood for the first time via explicit demonstration that these observed abnormal features in the trends of these two terms are indeed the manifestation of the crosstalk effect. With the crosstalk correction fully applied, both the calibration coefficients including the two minor terms and the linear term as well as EV retrievals for the band 30 are significantly improved. In addition, the fully corrected imagery for the bands 27–29 also shows further improvement superior to our previous

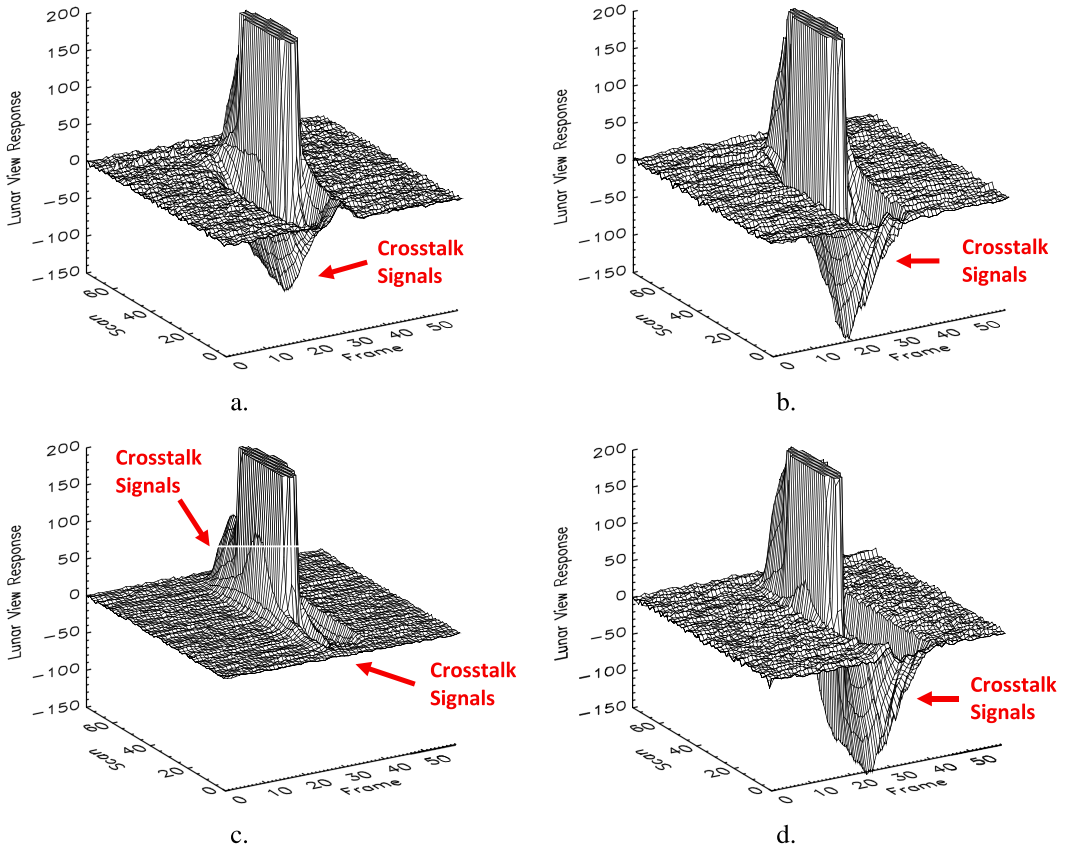

Figure 3. Lunar image observed by T-MODIS on 11 December 2014: (a) band 27 detector 3, (b) band 28 detector 3, (c) band 29 detector 3, and (d) band 30 detector 3.

results [*Sun et al.*, 2014a, 2014b, 2014c, 2015a, 2015b, 2015c] that use the noncorrected offset and linear term in the routine BB calibration and EV retrievals.

With the defined objective as stated above, the rest of the paper is prepared as follows. The next section details the crosstalk effect, algorithm, and the coefficients derived using the lunar view responses. The third section describes the WUCD calibration methodology and the crosstalk correction procedure to be applied on the corresponding WUCD data sets. The fourth section will show the improvements on the calibration coefficients derived from the WUCD events due to crosstalk correction. The fifth section shows the improvements of the crosstalk correction on EV retrievals by demonstrating the remarkable reduction of the striping with the crosstalk correction further applied to two minor terms, offset and nonlinear term. The crosstalk corrections on the offset and quadratic coefficients will rectify the radiometry of the affected bands, thereby achieving a complete correction over the entire dynamic range. Finally, the paper presents a summary of the work and future effort.

2. Crosstalk Effect, Algorithm, and Coefficients

Crosstalk is a complex phenomenon that comprises interference signals. The induction of electric signal is a convoluted noise that is transferred from various neighboring detectors on the same focal plane [*Sun et al.*, 2011, 2014a]. As the crosstalk is a convolved noise signal that has contributions from both the optical signal leak and the electronic setting of the circuitry, the effect is considered as one parameter. The periodic lunar observations of the MODIS provided a unique signal target that helped in identifying the additional crosstalk noise along with the Moon response. Based on a three-dimensional rendition of the Moon signal, it was easily discernible that the LWIR channels (bands 27–30) were affected by noise leak from the neighboring detectors. A few examples are shown in Figure 3. Figure 2 illustrates the exact location of the various detectors for the LWIR focal plane. The distances among the neighboring bands provide information to shift in the data

frame between the interference signals. Therefore, with the frame offsets known for each of the bands the source of the leaking signals is easily identified. The lunar surface plots observed on 11 December 2014 by detector 3 of bands 27–30, respectively, are shown in Figures 3a–3d. In order to better illustrate the crosstalk noise, the lunar responses are limited to a range of 200 dn. In actuality, the lunar responses could be as high as 4000 dn. From Figures 3a, 3b, and 3d, it can be seen that there is a slight protrusion downward in the shape of a valley near the cylindrical structure that represents the lunar response for bands 27, 28, and 30, respectively. However, in the case of band 29 (as shown in Figure 3c), there is a slight mound near the lunar response. This indicates that the contributions of the crosstalk effect could be either positive or negative and may also vary with time [*Sun et al*., 2014a, 2014b, 2014c, 2015a, 2015b, 2015c].

The crosstalk correction algorithm (details elaborated in *Sun et al*. [2014a]) is formulated using a linear function of the crosstalk contributors, and the contributions are additive. The integrated contribution of the crosstalk effect from the sending bands to a receiving detector D_r of a receiving band B_r is expressed as

$$dn^{\text{xtalk}}(B_r, D_r, F) = \sum_{B_s} C(B_r, D_r, B_s)\langle dn^{\text{msr}}(B_s, D_s, F + \Delta F_{\text{rs}})\rangle_{D_s}, \tag{1}$$

where B_s and D_s denote sending band and sending detector, respectively. $C(B_r,D_r,B_s)$ is the effective crosstalk coefficient from band B_s to band B_r and detector D_r, F is the frame number or pixel number along scan of B_r, ΔF_{rs} is the frame shift between band B_r and band B_s for viewing same target, $dn^{\text{msr}}(B_s, D_s, F + \Delta F_{\text{rs}})$ is the background subtracted measured instrument response of band B_s, detector D_s at frame $F + \Delta F_{rs}$, and the brackets indicate the average over the detectors of band B_s. It is assumed in equation (1) that the temperature of the scene changes smoothly along the track direction [*Sun et al*., 2014a]. In order to remove the crosstalk effect, the contribution of the leaking signals needs to be subtracted from the measured *dn* response. Then the correction needs to be applied at two places in the retrieval, the calibrator response and the EV response.

The crosstalk correction is based on the derived crosstalk coefficients that are representative of the magnitude contributions that need to be removed from the measured signal. The Moon surface and the surrounding background provide a sharp edge target to help identifying the extraneous noise [*Sun et al*., 2007]. The extraneous signals at the boundary of the lunar images are shown in Figure 3 and have been identified as the contamination of crosstalk from other bands [*Sun et al*., 2014a, 2014b, 2014c, 2015a, 2015b, 2015c, 2016]. This gives the magnitude of the contributions for the crosstalk. The crosstalk coefficients based on equation (1) are derived for the four bands (27–30) using the lunar responses. Since the Moon is not a homogenous surface, the sum of *dn* over scans for each detector for a complete lunar observation is used to derived the crosstalk coefficients. The procedure for deriving the crosstalk coefficients was described in detail in a previous work [*Sun et al*., 2014a]. It was also shown that the large extraneous signals in the summation were completely removed except for detector 8, which is still with extraneous signals although more than 90% reduced [*Sun et al*., 2014a]. A few examples of the crosstalk coefficients are illustrated in Figure 4. Figure 4a gives the long-term trend of the crosstalk coefficients for the affected band 27 from the sending band 29. These coefficients are inherently detector and time based. The coefficients for various detectors were positive in magnitude early on before gradually changing to a negative magnitude. The worst affected detector is detector 1 that had the largest change with significant drop starting in 2011. Also, the crosstalk contamination is significant from sending bands 28 and 30, although it is not shown here [*Sun et al*., 2014a, 2014c]. Examples for other crosstalk-affected bands such as band 28–30 are shown in Figures 4b–4d. As seen in the case of band 27, the crosstalk coefficients show very similar behavior, i.e., strong detector dependence and temporal drifts associated with sudden jumps [*Sun et al*., 2015a, 2015c, 2016]. In totality the crosstalk coefficients for each of four affected bands are modeled from the other three as the sending bands. Finally, it is assessed based on the coefficients that band 30 has the largest crosstalk impact, while band 29 was the least affected.

3. BB WUCD Calibration and Crosstalk Correction

For a MODIS TEB, the relationship between the at-sensor-aperture radiance L and the band's background subtracted instrument response *dn* is based on a quadratic fit

$$L = a_0 + a_1 dn + a_2 dn^2, \tag{2}$$

where a_0, a_1, and a_2 are the offset, linear term, and quadratic term, respectively [*Xiong et al*., 2009]. For MODIS TEBs, the unit of the radiance L is Watts/m^2/μm/steradian. Since *dn* is a unitless, all three coefficients a_0, a_1,

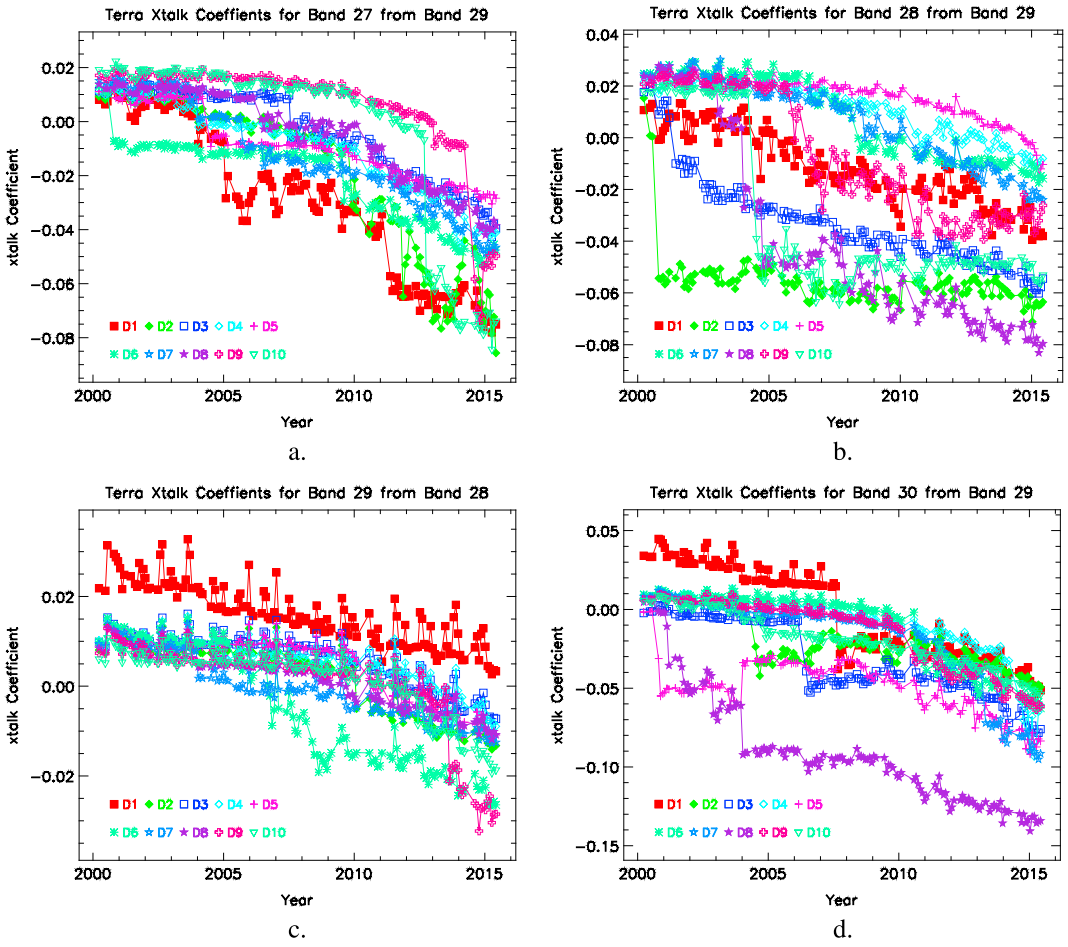

Figure 4. Illustration of T-MODIS EC coefficients for various receiving bands: (a) band 27 from band 29, (b) band 28 from band 29, (c) band 29 from band 28, (d) band 30 from band 29.

and a_2 have the same unit as the radiance. This is the unit used throughout this paper. For the BB calibration at the sensor radiance can be expressed as

$$L_{CAL} = RVS_{BB}\varepsilon_{BB}L_{BB} + (RVS_{SV} - RVS_{BB})L_{SM} + RVS_{BB}(1-\varepsilon_{BB})\varepsilon_{CAV}L_{CAV}, \quad (3)$$

where L_{CAL} is at the sensor aperture radiance for the BB view, RVS_{BB} (RVS_{SV}) is the response versus scan angle (RVS) at the sensor's BB (SV) view angle, ε_{BB} is the BB emissivity, ε_{CAV} is the effective scan cavity emissivity, and L_{BB} (L_{SM}, L_{CAV}) is the spectral radiance computed using Planck's equation at a measured T_{BB} (T_{SM} and T_{CAV}) [*Xiong et al.*, 2008, 2015]. From equation (2), the background subtracted instrument response dn_{BB} for BB observation can be related to the at-sensor-aperture radiance L_{CAL} by

$$L_{CAL} = a_0 + a_1 dn_{BB} + a_2 dn_{BB}^2. \quad (4)$$

For both Terra and Aqua MODIS, a BB WUCD process on a quarterly basis is implemented to derive the coefficients of the quadratic model, especially the offset and quadratic terms. In MODIS Collection 5 (C5) or earlier collections, equation (4) is fitted to the WUCD measurements without constraint. In MODIS C6 [*Wenny et al.*, 2012b; *Xiong et al.*, 2013], the offset term a_0 is constrained to be zero and only the linear and quadratic terms are fitted to the measured data. However, in the actual look up tables (LUTs), a_0 is kept zero for mirror side 1, while the offset for mirror side 2 takes the mirror side difference of the offsets, obtained via fitting without constraint, of the two mirror sides. This is an added fix to avoid the mirror side striping at low-temperature range [*Wenny et al.*, 2012b].

In a BB WUCD process, the BB is first cooled down to its ambient condition that is approximately close to 270 K. After this the BB heater is ramped up in a controlled step-wise pattern as shown in Figure 5. The BB

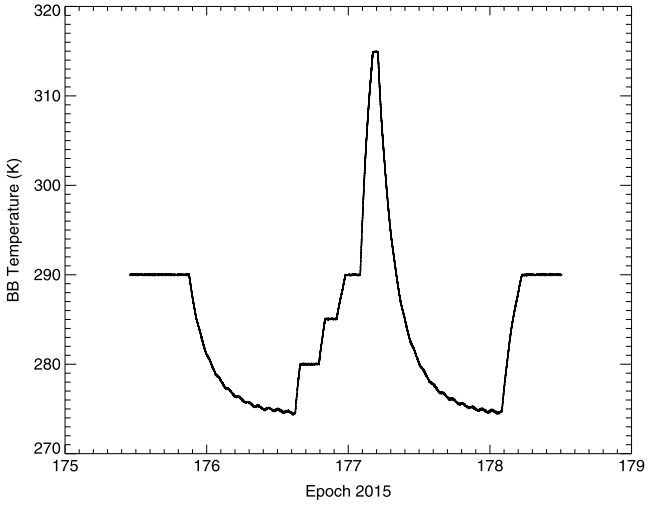

Figure 5. Illustration of a typical BB WUCD temperature profile, measured on 24–28 June 2015.

heater is switched off once the temperature reaches 315 K. The BB is then passively cooled in a slow fashion to its ambient temperature. The whole process takes about 2–3 days. Figures 6a–6d show an example illustrating the detector response versus the BB temperature from BB WUCD event on 25 June 2015 for bands 27–30. By fitting the measured instrument response and at the sensor aperture radiance calculated using equation (3) to the quadratic form described in equation (4), the a_0, a_1, and a_2 terms can be determined. In actual data processing, there are two choices, one using the warm-up data sets only, while the other using the cool-down data set only. In fact, there is a third choice to use both the warm-up and cool-down data sets to derive the calibration coefficients. In principle, the coefficients derived from the three approaches should be the same. Nevertheless, there are noticeable differences among the calibration coefficients derived from the three approaches. In this analysis, we use the approach employed in the

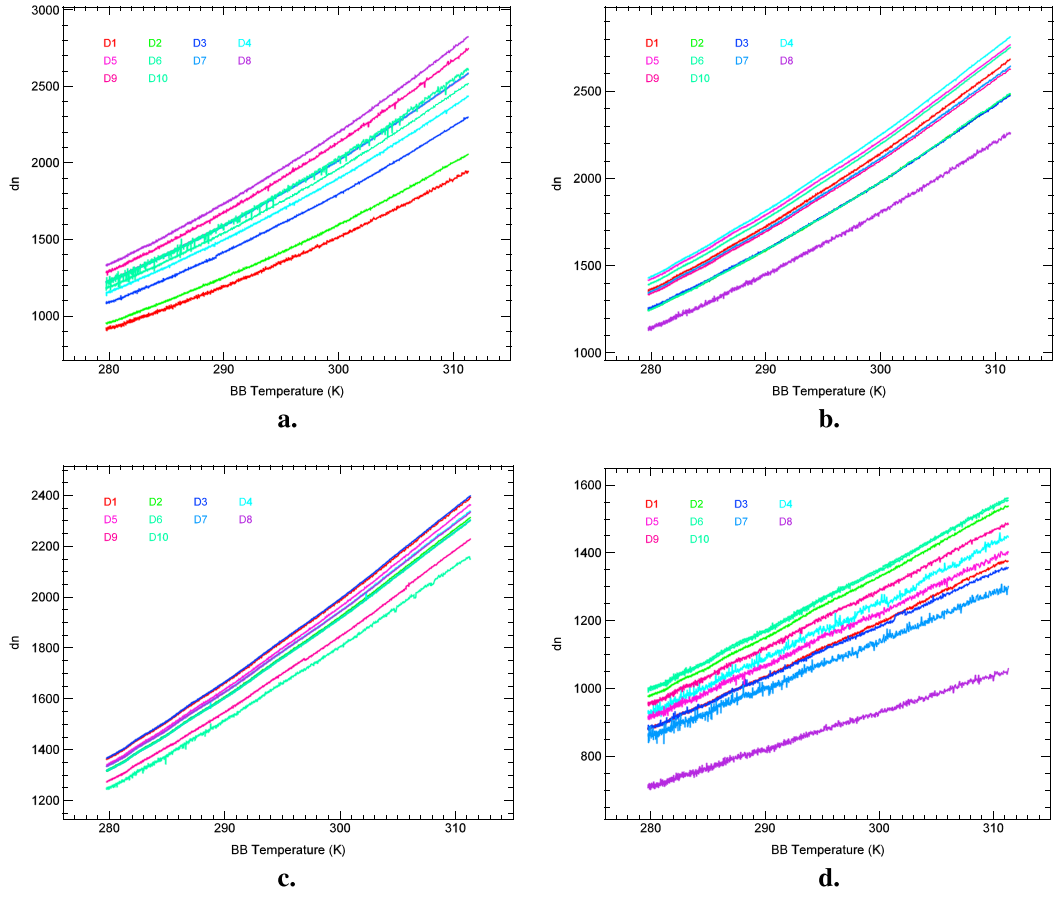

Figure 6. Detector responses versus BB temperature from WUCD event on 24–28 June 2015: (a) band 27, (b) band 28, (c) band 29, and (d) band 30.

current MODIS L1B C6, which is the most recent version of the MODIS L1B collections. For Terra MODIS C6, the calibration coefficients a_0 and a_2 for all TEBs, bands 20–25 and 27–36, were derived from BB cool-down event (315 K–270 K). The rationale behind this being that the above mentioned fitting strategy tended to be correct for cold scene biases, compared to the ones used in Collection 5 (C5) [*Wenny et al*., 2012a; *Xiong et al*., 2015]. Thus, for the rest of the discussions in this paper the cool-down data sets will be analyzed. Results for the warm-up process are very similar and left out for convenience.

In Terra MODIS C6, dn_{BB} represents the directly measured background subtracted instrument response for the BB view for all TEB, except for LWIR photo conductive (PC) bands 31–36. For the LWIR PC bands, there is an optical leak from the sending band 31. For these bands, a correction is applied in L1B C6 to remove the effect of the optical leak to obtain the corrected dn_{BB} [*Xiong et al*., 2003]. From the quarterly WUCD measurements, the coefficients, a_0, a_1, and a_2, of the quadratic model are derived and updated. In between two consecutive WUCD measurements, the BB temperature is nominally controlled at 290 K and thus the three calibration coefficients cannot be updated simultaneously. During each of the in-between time period, the offset a_0 and the quadratic term a_2 are fixed as constants, while the linear term is updated on a scan by scan using the following equation

$$b_1 = \left(L_{CAL} - a_0 - a_2 dn_{BB}^2\right)/dn_{BB}, \tag{5}$$

which is a different format of equation (4) and where linear term is denoted as b_1 instead of a_1 to distinguish the corresponding temperature-controlled status of the BB and also to distinguish the routinely updated linear term from one obtained from a WUCD event [*Xiong et al*., 2008]. In principle, the linear term b_1 derived on a scan-by-scan basis with the BB temperature controlled and linear term a_1 derived from the WUCD measurements should match. However, nonnegligible differences may be observed due to various reasons such as crosstalk contamination.

The measured instrument response for a TEB is contaminated with the crosstalk signal described in equation (2) when there is crosstalk from other bands on same FPA and the crosstalk effect is not negligible. Then contamination should be removed in both calibration and EV retrieval as previously mentioned. For the BB calibration, the sensor response with the removal of crosstalk signal can be written as [*Sun et al*., 2014a]

$$dn_{BB.}^{corrected}(B,D,F) = dn_{BB}^{msr}(B,D,F) - dn_{BB}^{xtalk}(B,D,F) \tag{6}$$

where $dn_{BB}^{corrected}(B,D,F)$ is the corrected instrument response for band B, detector D, and frame F. $dn_{BB}^{msr}(B,D,F)$ is the actual measured background subtracted instrument response for the band, detector, and frame. The crosstalk correction has been successfully applied in the BB calibration to remove the crosstalk effect in the derived linear term b_1 as well as in EV retrieval with the application of the corrected b_1 to remove the crosstalk impact in the MODIS L1B EV products. In this analysis, we focus on the crosstalk impact on the BB WUCD calibration, its effect on the derived offset a_0 and quadratic term a_2, and the removal of the crosstalk effect on the two coefficients. The crosstalk effect in the derived calibration coefficients can be removed by applying $dn_{BB}^{corrected}(B,D,F)$ described in equation (6) instead of $dn_{BB}^{msr}(B,D,F)$ used in the current C6 to refit the quadratic model in equation (4). The next section will show the improvements seen in the fitted calibration terms.

The impact of the crosstalk effect on the linear term b_1 comes from two sources, the crosstalk effect on offset a_0 and quadratic term a_2 and crosstalk contamination in the instrument response. In other words, both the crosstalk effect corrected a_0 and a_2 and the crosstalk corrected BB instrument response $dn_{BB}^{corrected}$ should be applied in equation (5) to fully correct the crosstalk effect on b_1. For EV radiance, the crosstalk contributions are from crosstalk effect on all three coefficients, a_0, b_1, and a_2, and crosstalk contamination in EV instrument response. To remove the crosstalk effect in EV radiance, the crosstalk corrected a_0 and a_2, fully corrected b_1, and the crosstalk corrected EV instrument response should be applied in the EV radiance formula to calculate the EV radiance. In our previous investigations on Terra bands 27–29, the crosstalk correction was not applied to a_0 and a_2 and the noncorrected a_0 and a_2 were applied to routine BB calibration and EV radiance calculation. As mentioned previously, the crosstalk correction remarkably improves the linear term b_1 and the EV L1B products for these three bands even though the crosstalk correction was not complete. This is because the crosstalk effect on a_0 and a_2 for these bands is relatively small and that the effect of the linear term is dominant. This will be discussed further in the next section. For the Terra band 30, full

crosstalk correction has been applied to both BB calibration and EV retrievals and it was shown that the crosstalk correction to a_0 and a_2 would be necessary in order to rectify the high quality and accuracy of the L1B products. In section 5, the improvements of the EV imagery by applying the crosstalk correction to a_0 and a_2 in addition to the application of the crosstalk correction to b_1 and EV instrument response will be shown to completion of this analysis. In the section, it will also be shown that the EV imagery for other LWIR PV bands is further improve by applying the crosstalk correction to a_0 and a_2.

4. Improvements of the Calibration Coefficients

In this section we discuss the impact of the crosstalk correction on the BB WUCD data sets under different settings. Roughly 60 data sets over the mission lifetime are available, and we process all using the approach described in section 3. Also, as mentioned earlier the analysis uses the BB cool-down data sets, which are the same data sets currently used for updating a_0 and a_2 in the operational MODIS C6 L1B products. Two fitting approaches, one with the constraint that the offset a_0 equals zero while the other without the constraint, are considered in fitting equation (4) to the measured data. As mentioned in the previous section, the current C6 methodology employs a second-order fitting with the offset set to zero, whereas the C5 methodology was a free quadratic fit. Both approaches are used in this analysis. It is worth to mention that a_0 should equal to zero according to equation (2) since *dn* becomes zero when *L* approaches zero. In fact, the Terra MODIS C5 L1B has shown insensitivity in capturing the cold scene temperatures, while the C6 L1B can provide better cold scene retrievals.

This paragraph describes the offset term fitted with equation (4) without constraint. Although the MODIS C6 TEB calibration coefficients are obtained under constrained fit, the final offset term for mirror side 2 is separately obtained under the unconstrained condition to account for the difference from mirror side 1. Figure 7a is the band 27 mirror side 1 a_0 without crosstalk correction, which goes up with time. Figure 7b is the band 27 mirror side 1 a_0 with the crosstalk correction, which becomes flatter. Figures 7c and 7d show a_0 mirror side differences without and with the crosstalk correction for the band 27. The two charts are very similar, and this is consistent with the expectation that the mirror side difference is not dependent on the crosstalk effect. From Figures 7a and 7b, it is seen that the a_0 term has trended in a slow fashion, with a slight upward tilt starting 2010. This is consistent with the previously reported crosstalk contamination [*Sun et al*., 2014a, 2014c]. However, after the crosstalk correction, the a_0 term is essentially constant at a small value about 0.05 for most detectors in band 27 with variability of approximately ±0.001 throughout the lifetime. This indeed is expected if the crosstalk effect is dominant and is properly characterized. This free fit result for the mirror side difference is the separate determination used to set the final nonzero offset term of mirror side 2 and is otherwise not used for the determination of a_1 and a_2 under constrained fit. We reiterate again that we are following the MODIS C6 procedure to obtain the mirror side 2 offset term, but here the main difference is that the electronic crosstalk correction has been applied.

For a_1 and a_2, we obtain four sets of value from the two different fitting conditions, one with the constraint that a_0 is forced to be zero while the other without, and also for before and after crosstalk correction. Careful comparisons first show that the two different fitting conditions do not generate coefficients that are impactfully different, although the constrained case shows very slightly improved stability. In reality the two mirror sides do have very small difference coming from other effects, but for this analysis the difference it is of little concern. From this point on in presentation, we only consider the case with a_0 constrained to zero to discuss results from before and after crosstalk correction.

Figure 8 gives the lifetime trend of the linear and quadratic calibration terms a_1 and a_2 for band 27. These are derived using the aforementioned data sets before and after the crosstalk correction. From Figure 8a, it is noticed that the linear term a_1 for the various detectors has trended slightly differently with the largest change observed for detectors 1 and 2. Also, the apparent disparity in the a_1 for the various detectors is reflective of the fact that the detector responses are not completely balanced as expected since they are basically of the same electronic circuitry. With the crosstalk corrections applied, these detector-to-detector differences in a_1 are significantly reduced and the remaining differences are primarily due to the electronic offsets of the individual detectors, which can be seen since the beginning. Consistent with our previous work, the long-term upward drifts, which are noticeable before the crosstalk correction, are significantly removed.

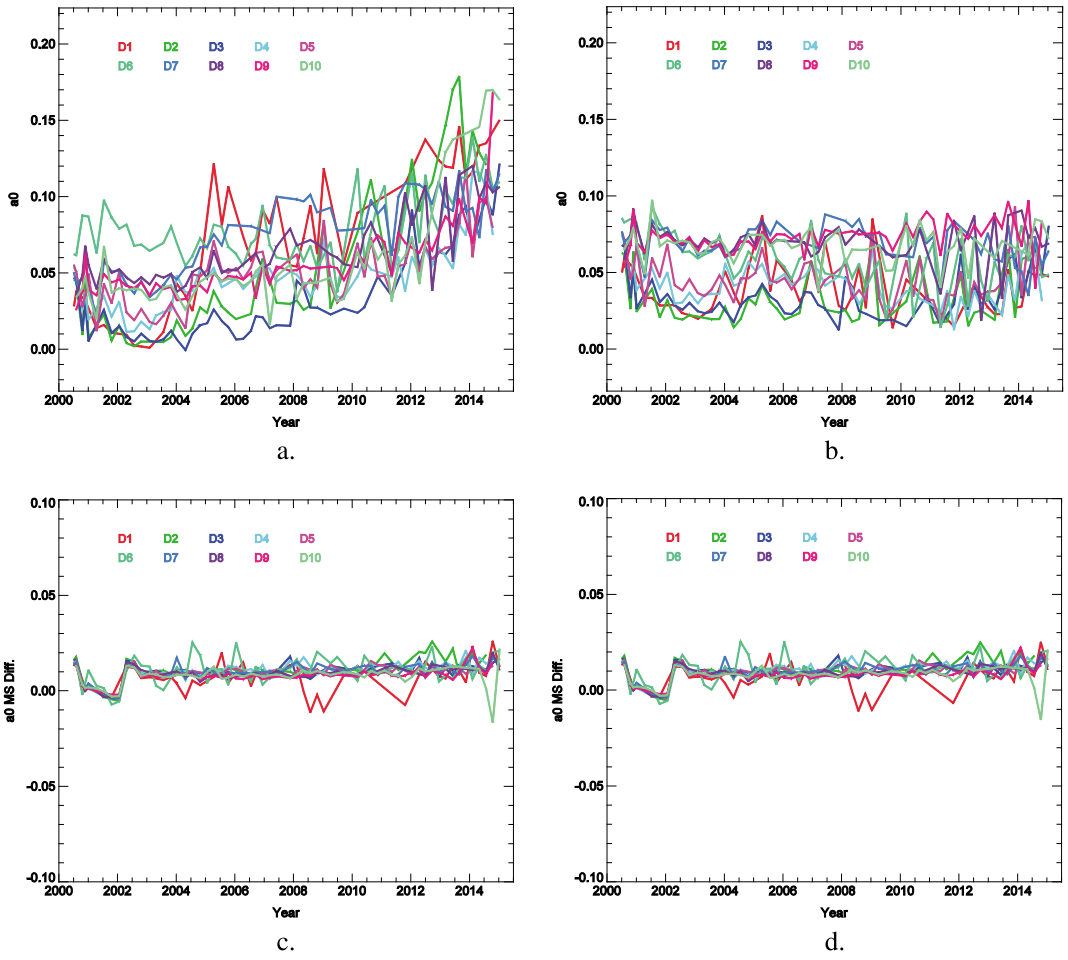

Figure 7. Calibration offset terms obtained from the fitting without the constrain that a_0 is kept 0 before and after the EC correction: (a) band 27 a_0 (before), (b) band 27 a_0 (after), (c) band 27 a_0 mirror side difference (before), and (d) band 27 a_0 mirror side difference (after).

These are well illustrated through Figure 8b. Finally, the higher quadratic term a_2 is analyzed. A compensation of the a_2 magnitude is observed before and after the crosstalk correction (illustrated by Figures 8c and 8d), which would ensure that the radiometry of the responses is well accounted for at the higher end of the instrument dynamic range.

Similar results to the band 27 are seen for band 28 in Figure 9. Figures 9a and 9b compare the a_1 term before and after the crosstalk correction. As with the case of the band 27, the a_1 term for the various detectors is improved on two counts. First, the long-term upward drift is reduced for all the detectors. Second, the detector responses are well equalized, thereby reducing the detector-to-detector differences [*Sun et al.*, 2015a, 2015c]. Finally, the nonlinear higher-order term a_2 is also corrected and is reduced in magnitude for the various detectors, in particular, for detectors 2 and 8. Consistent with the a_0 and a_1 trends, the variability of the a_2 term for all the detectors is also reduced considerably. These are illustrated through Figures 9c and 9d.

Moving on to the band 29, Figures 10a and 10b illustrate the a_1 trends before and after the crosstalk correction. Detectors 6, 7, and 9 have the largest change before and after the crosstalk correction. Consistent with the results previously reported [*Sun et al.*, 2015c], the a_1 trends are quite similar as the large long-term drifts and the within detector variability is both significantly reduced. The a_2 trends both before and after the crosstalk correction as shown in Figures 10c and 10d are in synchronization with the behavior observed in the band 28. It is noted that in the case of band 29, detector 6 is the maximally affected in terms of both the gain and noise [*Sun et al.*, 2015c]. Significant improvements are noted for this particular detector after the crosstalk correction.

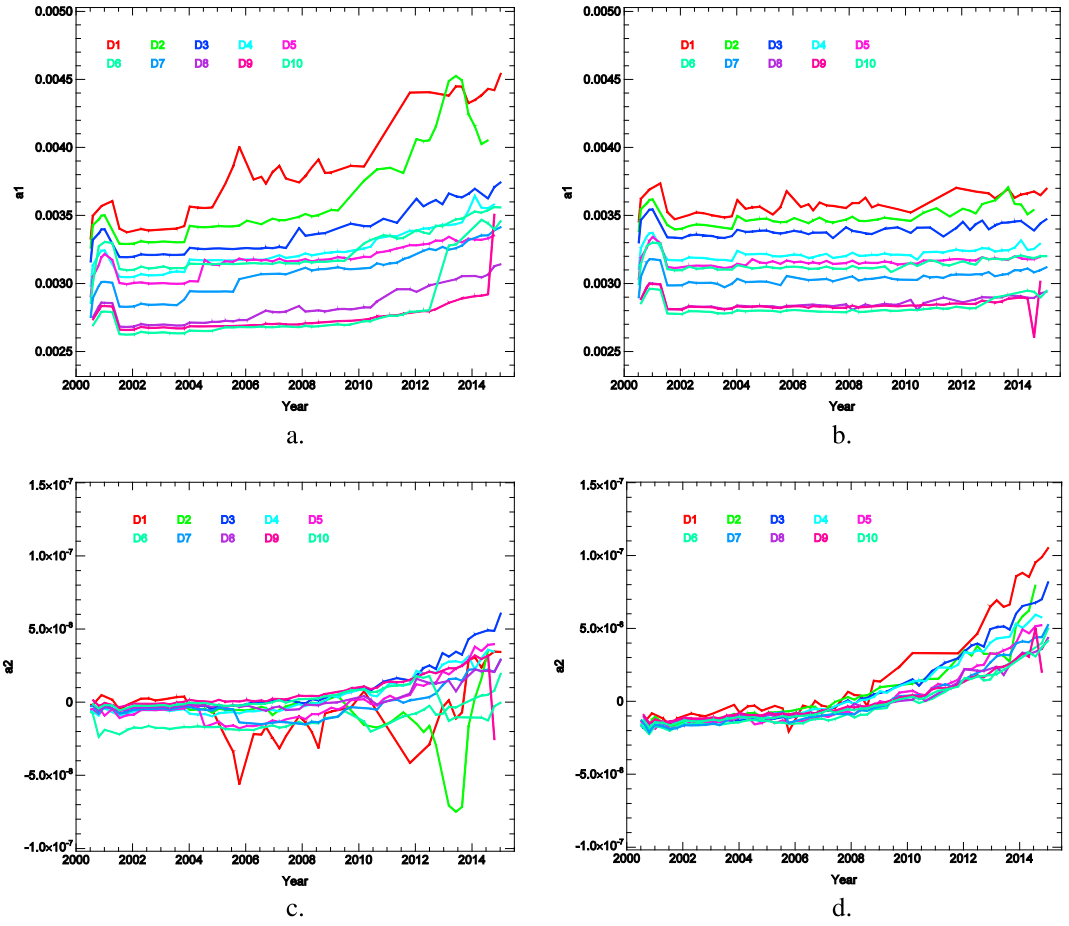

Figure 8. Calibration linear and nonlinear terms before and after the EC correction for band 27: (a) a_1 (before), (b) a_1 (after), (c) a_2 (before), and (d) a_2 (after).

At the time of the completion of this paper, the work on the band 30 has been published [*Sun et al.*, 2016]. Here we include some results that are also fully discussed in the band 30 analyses. Finally, the results for the band 30 are presented in this paragraph. Figures 11a and 11d summarize the impacts on the calibration terms a_1 and a_2 before and after the crosstalk correction. From the trends shown in Figures 11a–11d, two detectors 8 and 9 behave in a noisy fashion. In fact, detector 8 has been classified to be an out of family detector in the quality assurance flag in the L1B product. However, the crosstalk correction successfully removes these artifacts. From the a_1 trends shown in Figures 11a and 11b, it is quite clear that the apparent detector-to-detector disparity is considerably removed leading to a well-equalized a_1 trend after the crosstalk correction. Most importantly, the a_2 trends show a definite crosstalk contamination effect on the detector 8 responses. Referring to Figures 11c and 11d, it is very evident that this detector had the largest change starting 2001 and has significantly increased to at least 4 times larger in magnitude. A large change is observed for detector 8 later in the mission where the a_2 term spikes to as high as 4×10^{-6}, which is at least a magnitude larger than those shown in Figures 8–10 for bands 27, 28, and 29. After the correction (Figure 11d), the a_2 trend for detector 8 and other detectors seem to be well equalized and stable over the lifetime. They are also significantly reduced by a factor ranging from 2 to 10. Comparing Figures 8–11, it can be seen that the crosstalk effect has much larger impact on the a_2 of band 30 than on that of other bands.

Overall, Figures 8–11 demonstrate that the unexpected abnormal features in the a_0 and a_2 terms of the four LWIR PV bands, derived from the WUCD calibration without the application of the crosstalk correction, are mainly induced by the crosstalk contamination among themselves. This is first time that the source of this long-standing issue is understood and that a solution has been provided. From Figures 4 and 6, it can also be understood that why a_0 and a_2 of the band 30 would have the largest impact by the crosstalk effect—it is

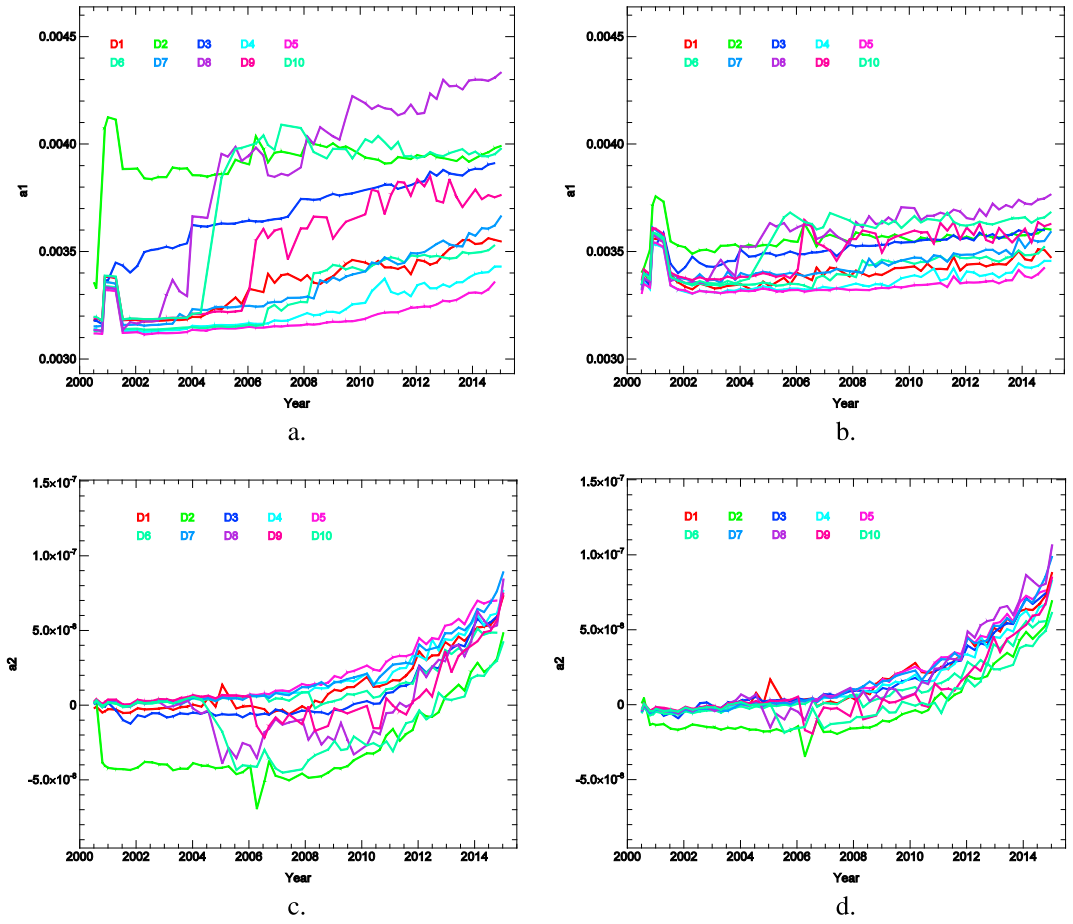

Figure 9. Calibration terms before and after the EC correction for band 28: (a) a_1 (before), (b) a_1 (after), (c) a_2 (before), and (d) a_2 (after).

because the band 30 not only has the largest crosstalk coefficients but also its crosstalk sending bands have much larger instrument responses during the WUCD calibration. This combination, as the effect multiplies as shown in equation (1), along with the band 30 responses being twice as small, resulted in the largest percentage of error for the band 30 in its a_0 and a_2 coefficients.

5. Improvements in EV Imagery

In this section, we discuss the impact of the crosstalk correction on the EV retrievals via three sets of data. The first set is from the MODIS C6 L1B [*Wenny et al.*, 2012b; *Xiong et al.*, 2013] which is without any electronic crosstalk correction at any level. The second set is with the crosstalk correction applied to routine BB calibration and EV retrievals but not to BB WUCD calibration [*Sun et al.*, 2014a, 2014b, 2014c, 2015a, 2015b, 2015c]. The third set is with crosstalk correction fully applied at all levels: apply the crosstalk correction in BB WUCD calibration first to obtain the corrected a_0 and a_2, then use the corrected a_0 and a_2 and apply the crosstalk correction (equation (6)) again in routine BB calibration to obtain corrected $b1$, and finally use the corrected a_0, a_2, and b_1 and apply the crosstalk correction (equation (6)) one more time in MODIS C6 L1B to produce EV retrievals. For the band 30, the detailed analysis and comparison of the three sets of data has already been reported [*Sun et al.*, 2016]. Here we focus on the improvements in EV imagery and show the importance of the crosstalk correction to a_0 and a_2 in rectification of the L1B products for Terra MODIS LWIR PV bands.

Figure 12a shows the measured band 30 EV images and profiles along track on 16 July 2012 at site near Baja Peninsula. Figure 12b is the C6 L1B brightness temperature BT with crosstalk correction applied but offset and nonlinear term. Figure 12c is the BT with crosstalk correction fully applied. The striping is clearly seen

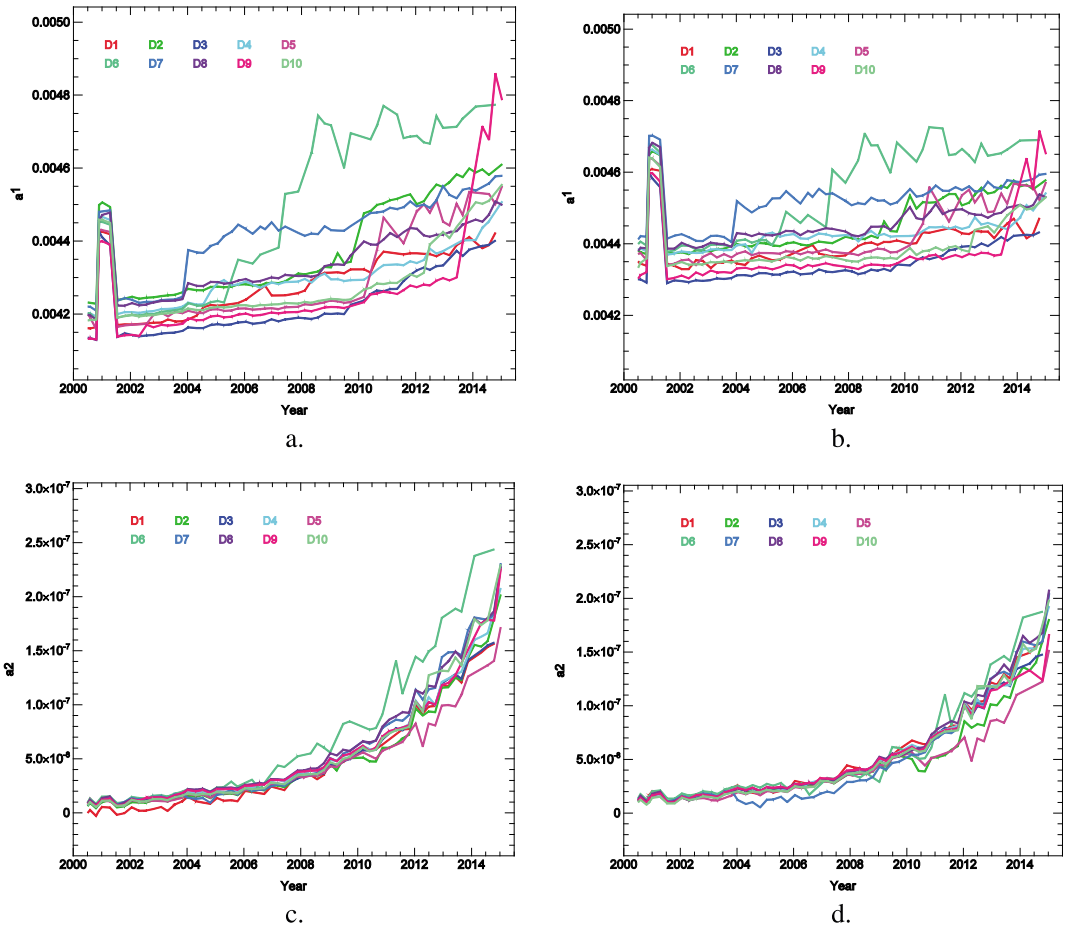

Figure 10. Calibration terms before and after the crosstalk correction for the band 29: (a) a_1 (before), (b) a_1 (after), (c) a_2 (before), and (d) a_2 (after).

in the C6 image, and the striping becomes even stronger when the crosstalk correction is only applied to the linear term and the EV retrievals but not to the offset and nonlinear term. Figure 12c shows the BT image after the crosstalk correction fully applied, in which the striping is almost perfectly removed. Figure 12d shows the BT profiles along track for the middle pixel along scan. To more clearly display the differences among the three curves in Figure 12d, the BT profiles with pixels numbers within 300 and 400 are enlarged and displayed in Figure 12e. Figures 12d and 12e confirm the aforementioned observations from Figures 12a–12c. The striping is about 4 K in original C6 L1B without the crosstalk correction, 8 K with the crosstalk correction applied to routine BB calibration ($b1$) but no crosstalk correction applied to WUCD calibration (a_0 and a_2), and less than 1 K with the crosstalk correction applied to all components, a_0, a_2, and b_1, and EV retrievals. This indicates that the application of the crosstalk correction to the WUCD calibration (a_0 and a_2) is vital for band 30 and has to be applied to the WUCD calibration in addition to the routine BB calibration (b_1) and the L1B EV retrievals. The significant striping reduction in the EV images is a direct demonstration of the improvement of the EV retrieval accuracy considering this mitigation comes from the very fundamental improvement in instrument calibration and not one of arbitrary image analyses. Thus, Figure 12 clearly demonstrates that the crosstalk correction is necessary for rectification of the quality and accuracy of the Terra band 30 L1B products [*Sun et al.*, 2016]. For the band 30, applying the correction only to the linear term cannot rectify the retrievals due to the acute impact of the nonlinear term. This demonstrates that the minor terms can become fundamentally important for some cases.

Figure 13 shows the similar BT images and profiles for band 27. Strong striping is clearly seen in Figure 13a. Figure 13b demonstrates that the crosstalk correction significantly reduces the striping and improves the quality of the image even though the correction is not applied to the offset and the nonlinear term. This is

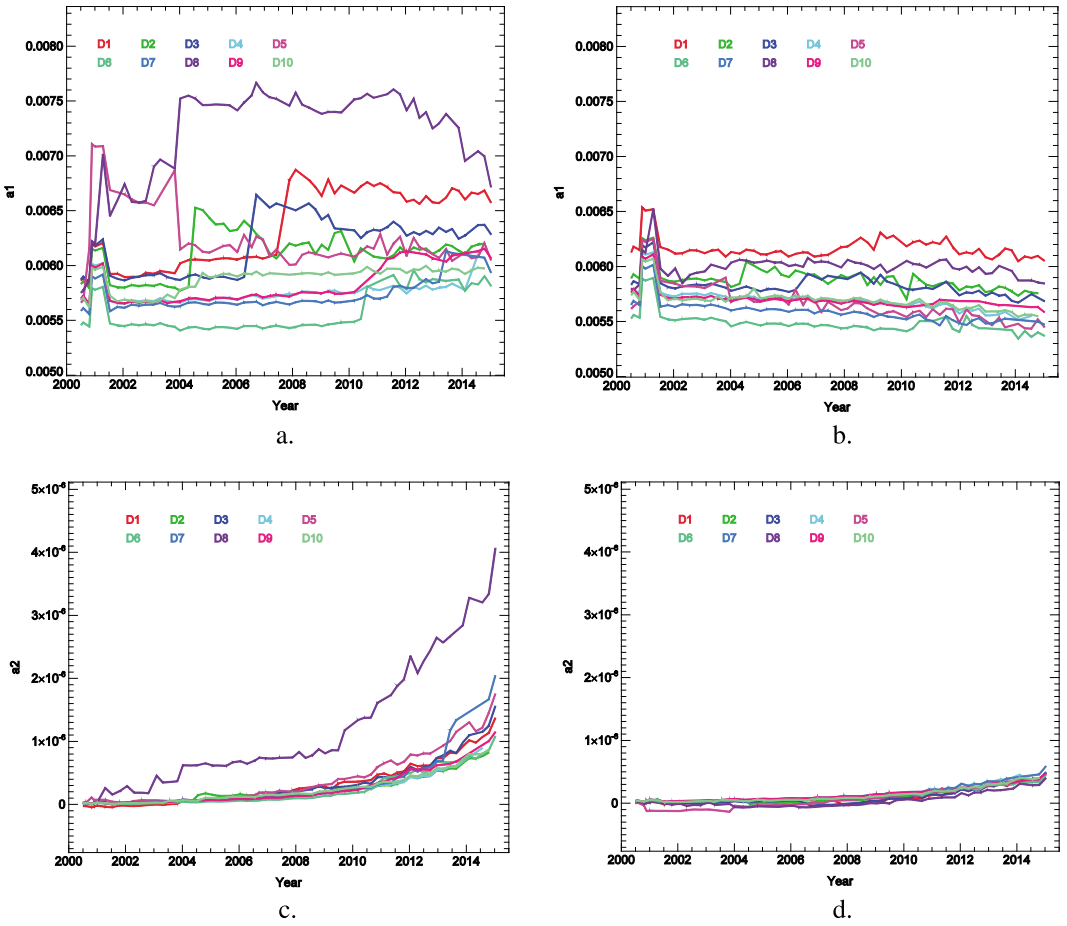

Figure 11. Calibration terms before and after the crosstalk correction for the band 30: (a) a_1 (before), (b) a_1 (after), (c) a_2 (before), and (d) a_2 (after).

expected and has been demonstrated in our previous work [*Sun et al.*, 2014a]. Figure 13c shows the BT image with the crosstalk correction fully applied. The striping is further reduced compared to that in Figure 13b. Figure 13d shows the BT profiles along track for the middle pixel along scan. Figure 13e is an enlargement of a subimage of Figure 13d to more clearly display the differences among the three profiles, same as Figure 12e for Figure 12d. They are consistent with the three images in Figures 13a–13c. The striping is reduced from about 10 K in original C6 L1B without the crosstalk correction to 2 K with the crosstalk correction but no crosstalk correction applied to a_0 and a_2, and further to 1.7 K with the crosstalk correction applied to a_0, a_2, and b_1, and EV retrievals. This indicates that the crosstalk correction applied to routine BB calibration (b_1) significantly reduces the striping, and the application of the correction to the WUCD calibration (a_0 and a_2) further improves the quality of EV imagery. As previously mentioned, this striping reduction due to the fundamental improvement in instrument calibration is a direct demonstration of the improvement of the EV retrieval accuracy. Figure 13 demonstrates that the impact of the crosstalk effect in the offset and nonlinear term on the L1B products is relatively small for the Terra band 27. This is also true for the bands 28 and 29. Considering their very similar performance compare to the band 27 and our focus on the WUCD calibration in this work, we elect not to show the BT images and profiles for the bands 28 and 29. The relative small impact of the crosstalk effect in the offset and nonlinear term on the L1B products is of different behavior from the band 30 that fully enters the nonlinear regime as explained in the previous section. This validates the results and conclusions in our previous investigations for the bands 27–29, in which the crosstalk correction was not applied to the offset and the nonlinear term and demonstrates that the linear term is indeed dominant [*Sun et al.*, 2014a, 2014c, 2015a, 2015c]. Nevertheless, the application of the crosstalk correction to the two minor terms further improves the quality and accuracy of the L1B products and should be included in future investigation or implementation of the crosstalk correction. It should be stated with

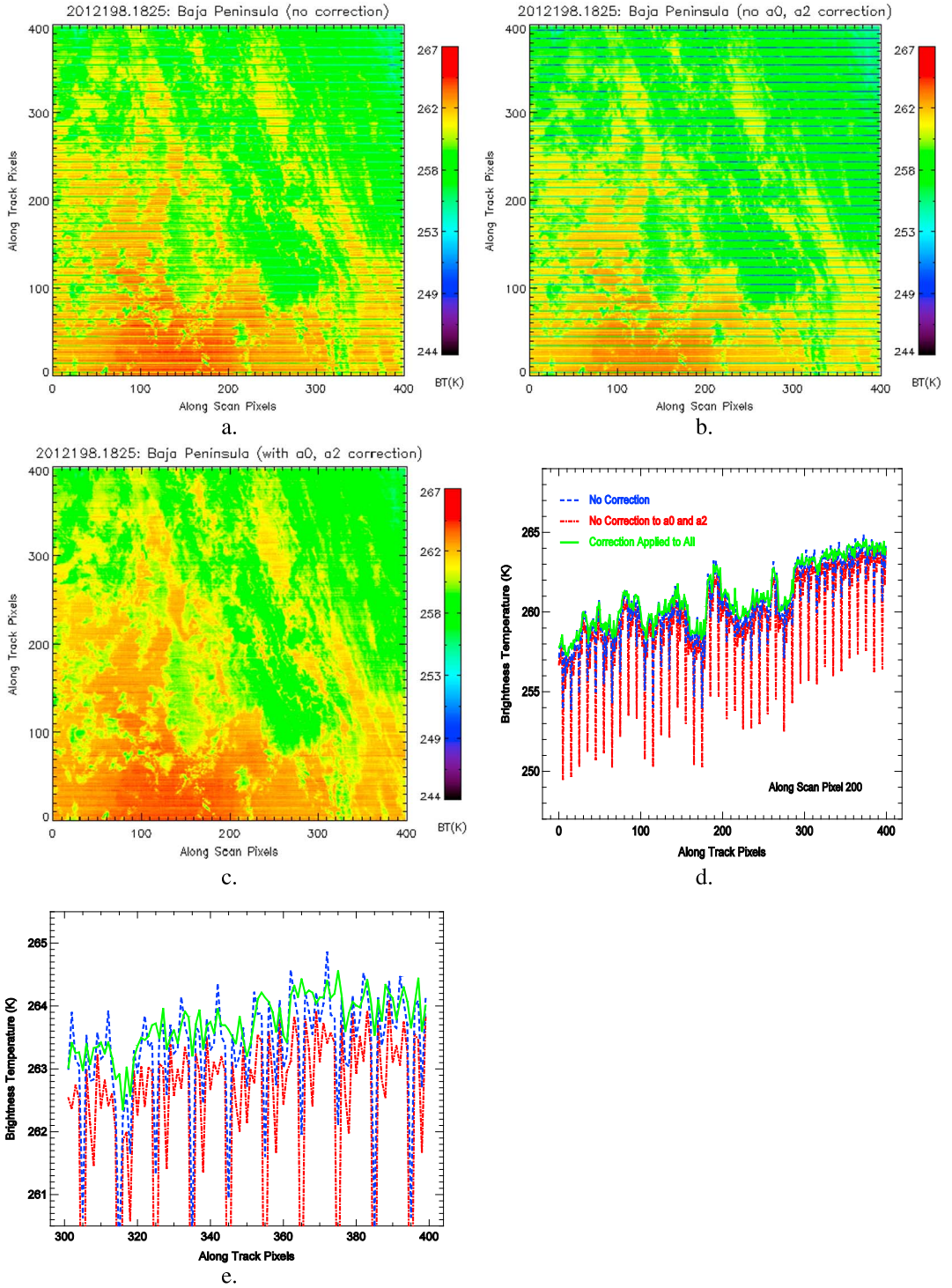

Figure 12. Crosstalk induced striping and the striping removal in BT of the Terra MODIS band 30 near Baja Peninsula in 2012: (a) C6 BT before the crosstalk correction; (b) C6 BT with the crosstalk correction but no crosstalk correction applied in a_0 and a_2; (c) C6 BT with the crosstalk correction applied to a_0, a_2, and b_1, and EV; (d) profiles along-track direction for all three cases; and (e) enlarge of the profiles in Figure 12d for the pixels with pixel number from 300 to 400.

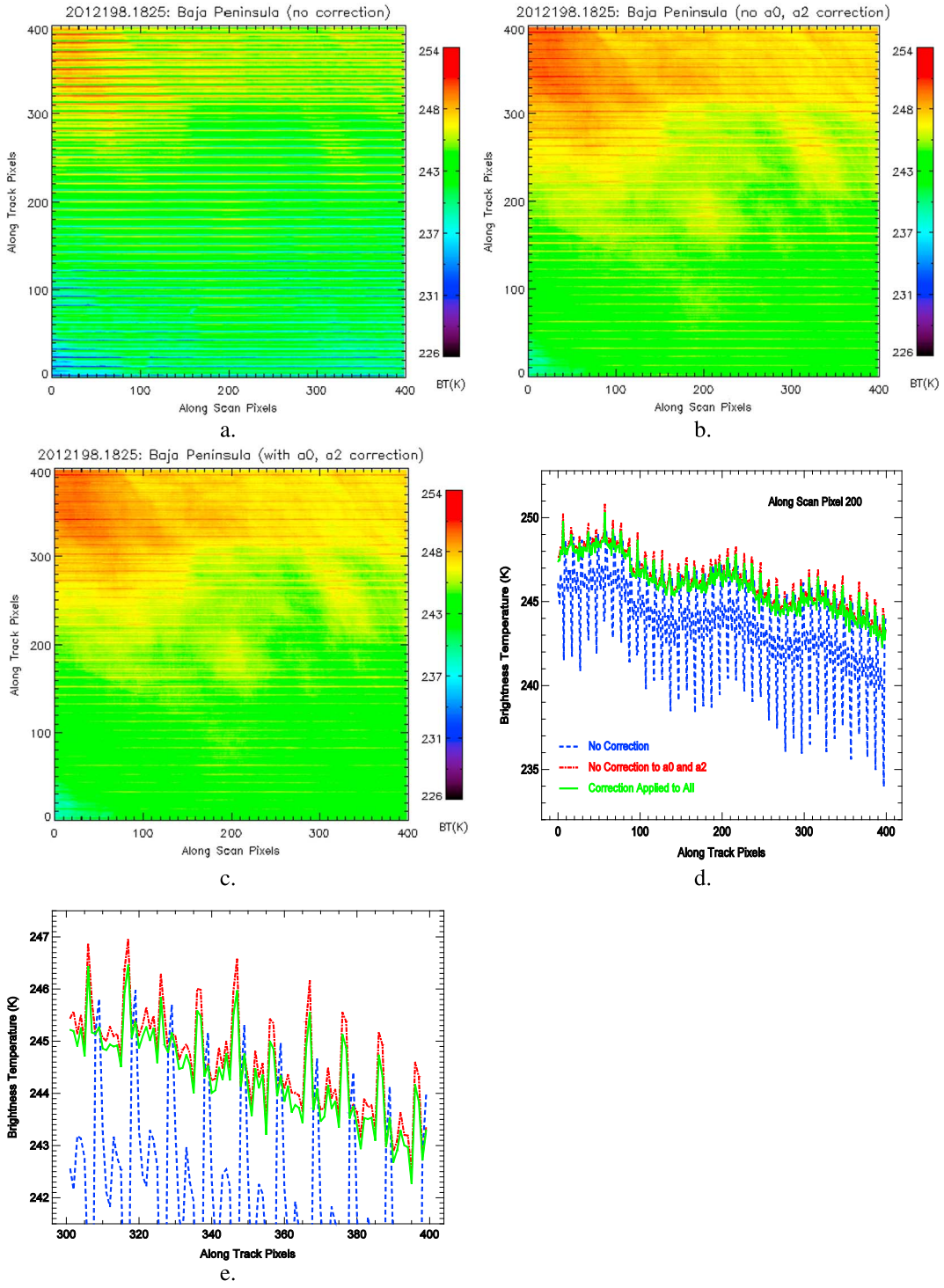

Figure 13. Crosstalk induced striping and the striping removal in BT of the Terra MODIS band 27 near Baja Peninsula in 2012: (a) C6 BT before the crosstalk correction; (b) C6 BT with the crosstalk correction but no crosstalk correction applied in a_0 and a_2; (c) C6 BT with the crosstalk correction applied to a_0, a_2, and b_1, and EV; (d) profiles along-track direction for all three cases; and (e) enlarge of the profiles in Figure 13d for the pixels with pixel number from 300 to 400.

caution that the crosstalk effect is continually evolving, and its impact on the nonlinear terms for the bands 27–29 may become significant in the future.

Overall differences among the three profiles are clearly seen in both Figures 12 and 13. It already has been established in our previous investigations [*Sun et al.*, 2014a, 2014b, 2014c, 2015a, 2015b, 2015c, 2016] that the crosstalk effect induces a long-term drift in EV brightness temperature besides striping. In other words, the crosstalk contamination induces radiometric errors as well. The errors become larger with time due to the increasing severity of the crosstalk effect [*Sun et al.*, 2014b]. The crosstalk contamination is also scene dependent due to the sending bands, as described in equation (1); and thus, the errors are scene dependent as well. Since the crosstalk correction removes or reduces the errors due to the crosstalk contamination, the overall differences among Figures 12a–12c and 13a–13c demonstrated in Figures 12d and 13d and Figures 12e and 13e, respectively, are expected and reflect the level of the radiometric improvement by the crosstalk correction.

Some striping still remains in both Figures 12c and 13c, where the crosstalk correction has been fully applied. The residual striping is about 1.7 K for the band 27 and less than 1 K for the band 30. The remaining striping can be induced by other reasons as well. For example, MODIS reflective solar bands also have strong striping but without the crosstalk effects. In other words, numerous errors can cause striping. As shown in our previous investigations [*Sun et al.*, 2014b, 2015a, 2015c, 2016], differences among the brightness temperatures obtained by different detectors are strongly seasonal dependent and increase with time before crosstalk correction. After crosstalk correction, they are not only significantly reduced as shown in Figures 12 and 13 but also become seasonal independent and time independent. This is an indication that the remaining striping may be induced by other mechanisms. Further investigation for the cause of the remaining striping and improvements of the TEB calibration method is needed, but they are beyond the scope and the purpose of this work.

Summary

We have shown that the correction for the crosstalk effect in WUCD is of fundamental importance to the four affected PV bands in Terra MODIS. Although previous investigations on bands 27–29 address only the linear calibration term, the new and the greater scope covered in this examination of WUCD establishes that the electronic crosstalk affects all four bands in the same fashion, although the manifestation may be band dependent. In bands 27–29 the crosstalk contamination in a_0 and a_2 is not critical, while in band 30 the correction for contamination in a_0 and a_2 is vital. It is remarkable that the linear theory and the correction algorithms work so well at all levels and over all conditions investigated. What we can understand is that crosstalk contamination is an underlying effect affecting these bands in exactly the same way and can be captured by a good model and be mitigated by a common algorithm despite complex and confusing manifestation in the instrument response. It is shown here that the sudden changes and all other unexpected abnormal features observed in the current C6 Terra MODIS PV LWIR bands (27–30) calibration coefficients, a_0, a_1, and a_2, of the TEB quadratic model are effectively removed by the crosstalk effect correction fully applied to all levels. Further, the crosstalk corrections on the minor calibration terms, i.e., a_0 and a_2, proved the effectiveness of the correction over the entire operating dynamic range of the instrument. The dramatic striping reduction in the EV imagery when crosstalk correction is fully applied to all levels provides the most direct proof that this complex phenomenon indeed has been properly characterized. As the MODIS Collection 6 is without electronic crosstalk correction, the implementation of the crosstalk correction in MODIS L1B is necessary and will significantly improve the image quality and the radiometric accuracy of the MODIS L1B retrievals, which will in turn improve the long-term science climate data. Additionally, the Visible Infrared Imaging Radiometer Suite (VIIRS) on board the Suomi National Polar-orbiting Partnership (SNPP) satellite has been on orbit for more than 4.5 years and has taken on the leading role as a major instrument. The crosstalk effect has been observed in its LWIR bands early in the mission even though it is much smaller than that observed in Terra MODIS LWIR PV bands [*Sun et al.*, 2012]. In fact, observable striping has been found in the SNPP VIIRS LWIR bands, thus indicating possible crosstalk effect. The methodology for crosstalk correction which we have developed can be applied to the SNPP VIIRS LWIR bands to improve the quality of the Sensor Data Records of these bands. The follow-up VIIRS instruments such as Joint Polar Satellite System (JPSS)-1, JPSS-2, etc. may also have crosstalk contamination, and the methodology can be applied to them as well.

Acknowledgments
We would like to thank Xiaoxiong Xiong and the MODIS Characterization Support Team (MCST) for support of this investigation. We would also like to thank Mike Chu for his helpful comments and suggestions. The MODIS L1A and OBC data used in this analysis are publicly available from NASA's LAADSWEB: https://ladsweb.nascom.nasa.gov/data/ and the MODIS BB WUCD information is available from the MCST's website: http://mcst.gsfc.nasa.gov/iot/weekly-reports. The views, opinions, and findings contained in this paper are those of the authors and should not be construed as an official NOAA or U.S. Government position, policy, or decision.

References

Barnes, W. L., and V. V. Salomonson (1993), MODIS: A global image spectroradiometer for the Earth Observing System, in *Critical Reviews of Optical Science and Technology*, vol. CR47, pp. 285–307.

Esaias, W. E., et al. (1998), An overview of MODIS capabilities for ocean science observations, *IEEE Trans. Geosci. Remote Sensing*, *36*, 1250–1265.

Guenther, B., X. Xiong, V. V. Salomonson, W. L. Barnes, and J. Young (2002), On-orbit performance of the Earth Observing System (EOS) Moderate Resolution Imaging Spectroradiometer (MODIS) and the Attendant Level 1-B data product, *Remote Sens. Environ.*, *83*, 16–30.

Justice, C. O., et al. (1998), The Moderate Resolution Imaging Spectroradiometer (MODIS): Land remote sensing for global change research, *IEEE Trans. Geosci. Remote Sensing*, *36*, 1228–1249.

King, M. D., W. P. Menzel, Y. J. Kaufman, D. Tanre, B. C. Gao, S. Platnick, S. A. Ackerman, L. A. Remer, R. Pincus, and P. A. Hubanks (2003), Cloud and aerosol properties, precipitable water, and profiles of temperature and water vapor from MODIS, *IEEE Trans. Geosci. Remote Sensing*, *41*, 442–458.

Madhavan, M. S., J. Sun, X. Xiong, B. N. Wenny, and A. Wu (2014), Statistical analysis of the electronic crosstalk correction in Terra MODIS band 27, *Proc. SPIE*, *9218*, 921,824.

Madhavan, S., X. Xiong, J. Sun, K. Chiang, and A. Wu (2015), Electronic crosstalk characterization of Terra MODIS long wave infrared channels, *Proc. SPIE 9607*, Earth Observing Systems XX, 9607–31.

Parkinson, C. L. (2013), Summarizing the first ten years of NASA's Aqua mission, *IEEE J. Sel. Top. Appl. Earth Obs. Remote Sens.*, *6*(3), 1179–1188.

Salomonson, V. V., W. L. Barnes, X. Xiong, S. Kempler, and E. Masuoka (2002), An overview of the Earth Observing System MODIS instrument and associated data systems performance, *Proceedings of IGARSS*.

Sun, J., X. Xiong, W. Barnes, and B. Guenther (2007), MODIS reflective solar bands on-orbit lunar calibration, *IEEE Trans. Geosci. Remote Sens.*, *45*, 2383–2393.

Sun, J., S. Madhavan, B. Wenny, and X. Xiong (2011), Terra MODIS band 27 electronic crosstalk: Cause, impact, and mitigation, *Proc. SPIE*, *8176*, 81760Z.

Sun, J., X. Xiong, and J. Butler(2012), NPP VIIRS on-orbit calibration and characterization using the Moon, *Proc. SPIE*, vol. 8510, pp. 85101I.

Sun, J., X. Xiong, S. Madhavan, and B. N. Wenny (2014a), Terra MODIS band 27 electronic crosstalk effect and its removal, *IEEE Trans. Geosci. Remote Sens.*, *52*, 1551–1561.

Sun, J., X. Xiong, Y. Li, S. Madhavan, A. Wu, and B. N. Wenny (2014b), Evaluation of radiometric improvements with electronic crosstalk correction for Terra MODIS band 27, *IEEE Trans. Geosci. Remote Sens.*, *52*, 6497–6507.

Sun, J., S. Madhavan, X. Xiong, and M. Wang (2014c), Electronic crosstalk correction for Terra long wave infrared photovoltaic bands, *Proc. SPIE*, *9264*, 926,412.

Sun, J., S. Madhavan, X. Xiong, and M. Wang (2015a), Investigation of the electronic crosstalk in Terra MODIS band 28, *IEEE Trans. Geosci. Remote Sens.*, *53*, 5722–5733.

Sun, J., S. Madhavan, X. Xiong, and M. Wang (2015b), Electronic crosstalk in Terra MODIS thermal emissive bands, *Proc. SPIE*, *9607*, 960,730.

Sun, J., S. Madhavan, X. Xiong, and M. Wang (2015c), Long-term trend induced by electronic crosstalk in Terra MODIS band 29, *J. Geophys. Res.: Atmos.*, *120*, 9944–9954.

Sun, J., S. Madhavan, and M. Wang (2016), Investigation and mitigation of the crosstalk effect in Terra MODIS band 30, *Remote Sensing*, *8*(249), 1–17.

Wenny, B. N., X. Xiong, and S. Madhavan (2012a), Evaluation of Terra and Aqua MODIS thermal emissive band calibration consistency, *Proc. SPIE*, *8533*, 853317-1–853317-9.

Wenny, B. N., A. Wu, S. Madhavan, Z. Wang, Y. Li, N. Chen, V. Chiang, and X. Xiong (2012b), MODIS TEB calibration approach in collection 6, *Proc. SPIE*, *8533*, 85331M.

Xiong, X., J. Sun, K. Chiang, S. Xiong, and W. L. Barnes (2003), "MODIS on-orbit characterization using the Moon", Proc. SPIE 4881, 299-307.

Xiong, X., K. Chiang, A. Wu, W. Barnes, B. Guenther, and V. Salomonson (2008), Multiyear on-orbit calibration and performance of Terra MODIS thermal emissive bands, *IEEE Trans. Geosci. Remote Sens.*, *46*, 1790–1803.

Xiong, X., B. Wenny, A. Wu, and W. Barnes (2009), MODIS on-board blackbody function and performance, *IEEE Trans. Geosci. Remote Sens.*, *47*.

Xiong, X., G. Toller, J. Sun, B. Wenny, A. Angal, and W. Barnes (2013), MODIS level 1B algorithm theoretical basis document, version 4, prepared for National Aeronautics and Space Administration.

Xiong, X., A. Wu, B. N. Wenny, S. Madhavan, Z. Wang, Y. Li, N. Chen, W. Barnes, and V. Salomonson (2015), Terra and Aqua MODIS thermal emissive bands on-orbit calibration and performance, *IEEE Trans. Geosci. Remote Sensing*, *53*, 5709–5721.